Journal of Power Sources 246 (2014) 39–48

Contents lists available at SciVerse ScienceDirect

Journal of Power Sources

journal homepage: www.elsevier.com/locate/jpowsour

Thermally stable polybenzimidazole/carbon nano-tube composites for alkaline direct methanol fuel cell applications

Jung-Fen Wu [a], Chieh-Fang Lo [a], Long-Yun Li [a], Hsieh-Yu Li [b], Chia-Ming Chang [c], Kuo-Sung Liao [c], Chien-Chieh Hu [c], Ying-Ling Liu [b,**], Shingjiang Jessie Lue [a,*]

[a] Department of Chemical and Materials Engineering, Chang Gung University, Kwei-shan, Taoyuan 333, Taiwan, ROC
[b] Department of Chemical Engineering, National Tsing Hua University, Hsinchu 300, Taiwan, ROC
[c] Department of Chemical Engineering and R&D Center for Membrane Technology, Chung Yuan University, Chung-Li 320, Taiwan, ROC

HIGHLIGHTS

- CNT causes high fractional free volume in a polymer matrix.
- Water diffusivities are enhanced in CNT-containing PBI films.
- GDEs without PTFE treatment give higher power density compared to commercial GDEs.
- DMAFC containing CNT electrolyte achieves a peak power density of 104.7 mW cm^{-2}.

ARTICLE INFO

Article history:
Received 3 April 2013
Received in revised form
27 May 2013
Accepted 28 May 2013
Available online 10 June 2013

Keywords:
Cell performance
Carbon nano-tube composites
Polybenzimidazole (PBI) electrolyte
Structure–property relationship

ABSTRACT

Nanocomposites of thermally stable polybenzimidazole (PBI) containing small amounts (<1%) of functionalized multi-walled carbon nano-tubes (CNT) are prepared using solution casting methods. These PBI and PBI/CNT composites are doped with potassium hydroxide (KOH) solution to prepare hydroxide-conducting electrolytes for alkaline direct methanol fuel cell (ADMFC) applications. The CNT-containing composites exhibit higher fractional free volumes and higher water diffusivities. CNT also promotes ionic conductivity of electrolytes and improves the fuel cell performance. Gas diffusion electrodes (GDEs) without polytetrafluoroethene (PTFE) treatment give superior cell power density compared to commercial E-tek GDEs, which contain hydrophobic PTFE layers. When the fuel cell is fed with 2 M methanol in 6 M KOH (as the anode fuel) and humidified oxygen (as the cathode oxidant), the system achieves a maximum power density of 104.7 mW cm^{-2} at 90 °C. These KOH-doped PBI/CNT composites have the potential to be used in high temperature alkaline fuel cell applications.

1. Introduction

Energy shortages have become the most important global issue of the 21st century. Scientists have been studying fuel cells as potential energy sources and have developed hydrogen fuel cell (also called proton-exchange membrane fuel cells, PEMFCs). Although a PEMFC has several advantages, such as a small footprint, quiet operation, high energy conversion efficiency, and low emission of carbon dioxide, it also has the drawbacks of requiring hydrogen fuel storage and low carbon monoxide tolerance [1]. Direct methanol fuel cells (DMFCs) are considered to be suitable power suppliers for portable and mobile devices. However, the high methanol cross-over rates observed when using perfluorosulfonic acid membranes, such as Nafion®, have resulted in fuel loss and reduced fuel cell voltage [2,3].

Tripkovic et al. found that the methanol oxidation rate is higher in an alkaline solution than in an acidic medium [4,5]. In an alkaline direct methanol fuel cell (ADMFC), the hydroxide ions are produced on the cathode by reacting oxygen with water vapor. The produced hydroxide ions then diffuse from the cathode to the anode, with in an opposite direction to the methanol fuel diffusion from the anode to the cathode. This intrinsic hydroxide ion diffusion can suppress the methanol cross-over [6,7]. In an ADMFC, it is possible to use non-platinum catalysts for the oxygen reduction reaction on the cathode [8,9]. With the advantages of fast reaction kinetics, suppressed methanol cross-over, and non-platinum catalysts, ADMFCs have received an increasing amount of attention over the last few years [10–12].

* Corresponding author. Tel.: +886 3 2118800x5489; fax: +886 3 2118700.
** Corresponding author. Tel.: +886 3 5715131x33651; fax: +886 3 5715408.
E-mail addresses: liuyl@mx.nthu.edu.tw (Y.-L. Liu), jessie@mail.cgu.edu.tw (S.J. Lue).

0378-7753/$ – see front matter © 2013 Elsevier B.V. All rights reserved.
http://dx.doi.org/10.1016/j.jpowsour.2013.05.171

Nomenclature

A	electrode working area, cm^2
D	water diffusion coefficient, $cm^2\ s^{-1}$
M	solvent uptake in membrane, $g\ g^{-1}$
L	KOH-doped electrolyte thickness, cm
M_t	solvent uptake in membrane at time t, $g\ g^{-1}$
M_∞	solvent uptake in membrane at equilibrium, $g\ g^{-1}$
R_E	electrolyte bulk resistance, Ω cm
t	time, s
W_o	membrane dry weight, g
W_t	membrane wet weight, g
δ	membrane thickness, cm
σ	conductivity of membrane electrolyte, $S\ cm^{-1}$

ADMFC performances (cell voltage and output power density) usually increases with temperature in the 30–100 °C range [7,13–15], making the development of thermally stable membrane electrolytes of critical importance. Zhou et al. developed polymer electrolyte (poly(vinyl alcohol)/poly(acrylamideco-diallyldimethylammonium chloride)/ethylene glycol [14] and Varcoe and Slade reported quaternary-ammonium-functionalized poly(ethylene-co-tetrafluoro ethylene) [15]) for ADMFC applications, with cell temperatures up to 70–80 °C. Moreover, polybenzimidazole (PBI) has been proposed as a thermally stable alternative; the material also has a higher mechanical strength and lower methanol permeability than Nafion [16]. Acid-doped PBI has been investigated in PEMFC and proton-exchange direct methanol fuel cells (DMFCs) [17–21]. For example, Lobato et al. doped PBI in a DMFC with phosphoric acid and obtained a peak power density of 138.5 mW cm^{-2} at 200 °C [18]. Wycisk et al. prepared a PBI-Nafion blend film and achieved 100 mW cm^{-2} at 60 °C when feeding 1 M methanol into a DMFC [19]. Long-term operation using PBI electrolytes, however, shows decay in performance with time. A voltage loss of at 43 mV h^{-1} was reported for phosphoric acid (H_3PO_4)-doped PBI operated in a PEMFC at 160 °C and 600 mA cm^{-2} for 1800 h [22]. A power loss of 0.7 mW cm^{-2} per cycle was observed over the first 60 daily cycles with H_3PO_4-doped PBI for a fuel cell fed with hydrogen and air at 150 °C and ambient pressure [23].

In light of the potentials for applying PBI in alkaline fuel cells, Hou et al. prepared potassium hydroxide (KOH)-doped PBI to fabricated alkaline methanol fuel cells and obtained a peak power density of 31.0 mW cm^{-2} at 90 °C [24]. For an alkaline direct ethanol fuel cell (ADEFC), peak power densities of 60.0–100 mW cm^{-2} were reported at 80–90 °C [25,26]. In addition, Pt-free air-breathing ADEFC with PBI/KOH membrane was able to output a peak power density of 16 mW cm^{-2} at 60 °C and this fuel cell was stably operated for 336 h above 0.3 V [27]. It has been reported that hydrogen bonding and/or neutralization may occur between KOH and PBI, promoting the ionic conductivity of KOH-doped PBI films [25,27].

In our previous publications, we reported the advantages of incorporating polymer-functionalized carbon nano-tubes (CNTs) into polyvinyl alcohol matrices for preparation of solid electrolytes for alkaline fuel cells. The polymer layer around the CNTs provided micro-channels for water and hydroxide ion transfers. The ionic conductivity was thereby further improved in the CNT-containing electrolytes [28–30]. Meanwhile, the fuel permeability was suppressed due to the steric hindrance of the CNTs [28,29,31]. The CNT incorporation has been shown to improve cell performance in both proton-exchange and hydroxide-conducting DMFCs [28,32,33].

In this study, multi-walled CNTs were functionalized with PBI and the resulting CNTs were incorporated into a PBI matrix. The physical, electrical, and transport properties of the PBI and PBI/CNT nanocomposites were evaluated. ADMFC performances employing the KOH-doped PBI-based electrolytes were determined. Key operating parameters for the cell operation were also optimized. The cell voltage and power density were correlated with the electrolyte characteristics to elucidate the effects of CNT addition into PBI on fuel cell performance.

2. Experimental

2.1. Materials

3,3-Diaminobenzidine (DAB, 99%, Sigma–Aldrich, St. Louis, MO, USA), isophthalic acid (IPA, 99%, Alfa Aesar, Heysham, Lancashire, UK), and polyphosphoric acid (PPA, ca. 84%, Alfa Aesar) were used as received. Sodium bicarbonate (99.5%) and ortho-phosphoric acid (85%, HPLC grade) were purchased from Showa Chemical Co. (Tokyo, Japan) and Scharlau Chemie (Barcelona, Spain), respectively. *N*,*N*-dimethylacetamide (DMAc) in HPLC grade was received from TEDIA and dried over 4 Å molecular sieves (Acros, Geel, Belgium) for at least 2 days before use. Multi-walled carbon nanotubes (MWCNT), with average diameters of 10–50 nm and lengths of 125 nm were obtained from the Carbon Nano-tube Co., Ltd., Incheon, Korea. The purity of the received MWCNT was 93%. MWCNT was washed with dimethylsulfoxide prior to use. KOH was obtained from Sigma–Aldrich. Methyl alcohol (HPLC grade, 99.9%) was from Acros Organics. Gas diffusion electrodes (GDEs) with 5 mg cm^{-2} Pt–Ru alloy (1:1)/C on carbon cloth for the anode and 5 mg cm^{-2} Pt/C on carbon cloth for the cathode were purchased from E-tek, Somerset, NJ, USA. Commercial platinum (Pt) black (40:60 atomic %, HiSPEC™ 1000) and Pt–Ru black (50:50 atomic %, HiSPEC™ 6000) were purchased from Johnson Matthey (London, UK). De-ionized (DI) water with resistivity of 18 MÙ cm was produced using a Millipore water purifier (Elix 5/Milli-Q Gradient system, Millipore Corp., Bedford, MA, USA).

2.2. PBI synthesis and preparation of PBI-functionalized MWCNTs

PBI was synthesized by a polycondensation reaction according to the methods described elsewhere [31]. Fifteen grams of DAB and 250 g of PPA were placed in a 1-L round bottom flask equipped with magnetic stirrer. The solution was heated to 140 °C under a nitrogen stream to dissolve the DAB in the PAA. 11.63 g of IPA was then added and the temperature was raised to 200 °C. After 15 h, the viscous solution was poured into a large amount of cold water. The formed fibers were kept in water for at least 3 days. The excess acid was then neutralized with a sodium bicarbonate aqueous solution (1 M). The polymer was then collected by filtration, washed thoroughly with water and methanol, and then dried under vacuum at 130 °C overnight. The synthesized PBI exhibited an inherent viscosity of 0.8–1.0 $cm^3\ g^{-1}$ in DMAc at 25 °C [33].

PBI-functionalized MWCNT was prepared using an ozone-mediated method as reported previously [33]. The pristine MWCNT was dispersed in PBI/DMAc solution and purged with ozone/oxygen gas. The treated MWCNT were collected, washed, and dried to produce PBI-functionalized MWCNT samples. The polymer grafting onto the MWCNT was confirmed using FTIR and Raman spectra, and the PBI-functionalized MWCNT contained 25 wt% of PBI [33].

2.3. PBI and PBI/CNT composite preparation

An appropriate amount of PBI polymer was dissolved in 22 g of DMAc and mixed for 3 h to form a homogeneous polymer solution. This solution was poured into a petri dish with a diameter of 9 cm

and dried in a vacuum oven at 120 °C for 8 h. The dry film was peeled from the petri dish and soaked in 500 mL of methanol solvent at 60 °C. The methanol solvent was changed every 3 h over a total of 12 h so that the methanol would replace the residual DMAc in the film. The film was then dried at 200 °C for 4 days.

The PBI-functionalized MWCNT was suspended in 5 g of DMAc by ultrasonication at room temperature for 8 h. The PBI solution in 17 g of DMAc was prepared according to the aforementioned procedure. The PBI-functionalized MWCNT suspension and PBI solution were mixed for an additional 2 h under ultrasonication and poured into a petri dish. The mixture was then dried. The film was then peeled from the petri dish, soaked in methanol, and dried again in a procedure similar to that for PBI preparation. The resulting PBI composites were referred to as PBI/CNT films and consisted of 0.05% (weight basis) of PBI-functionalized MWCNT, unless stated otherwise. The thickness of the dry composite membrane was 40–50 μm. The PBI and PBI/CNT composites were immersed in 6 M KOH solution for 24 h to form hydroxide-conducting electrolytes [29]. These KOH-doped PBI and PBI electrolytes were referred as PBI/KOH and PBI/CNT/KOH.

2.4. Characterization

Fourier transform infrared (FTIR) spectra of the functionalized CNT, PBI, and PBI/CNT composite membranes were obtained via the attenuated total reflectance method using an FTIR (Perkin Elmer Spectrum One, Perkin Elmer Corp., Norwalk, CT, USA) equipped with a multiple internal reflectance apparatus and a ZnSe prism as an internal reflection element. Thermo-gravimetric analysis (TGA) was performed on the PBI and PBI/CNT composites using an analyzer (TA-TGA Q-500, TA Instrument, New Castle, DE, USA) under a nitrogen atmosphere at a heating rate of 10 °C min^{-1}. The dry and swollen masses of the KOH-doped electrolytes were also recorded to reveal the water and KOH sorption levels inside the electrolytes using a gravimetric procedure reported previously [29]. The membrane micro-structure was observed using field-emission scanning electron microscope (FE-SEM, model S-4800, Hitachi High-Technologies Corp., Tokyo, Japan) after samples were freeze-fractured in liquid nitrogen and sputtered with Pt. An X-ray diffraction (XRD, model D5005D, Siemens AG, Munich, Germany) measurement was performed on PBI and PBI/CNT composite membranes to examine their crystalline characteristics. The X-ray radiation was generated using Cu Kα (wavelength 1.54056 Å) from an anode operating at 40 kV and 40 mA. The scanning rate was 5° s^{-1}. The XRD was recorded for angles ranging from 10 to 80° [28,34]. The water contact angles on the membranes were measured using a contact angle measurement system (G10-MK2, Kruss GmbH, Hamburg, Germany) equipped with a V2:RS170 camera (North American NTSC standard, 60 Hz) and analyzed with FTA32 software. The mechanical property of the membranes (which were cut into dumb-bell shape specimens with lengths of 25 mm and widths of 5 mm) was measured with a Sintech machine (Sintech 5/G, MTS Systems Co., Ltd. Eden Prairie, MN, USA) with an elongation rate of 10 mm min^{-1} at ambient temperature. Positron annihilation lifetime spectroscopy (PALS) was used to analyze the fraction free volume present in the moistened PBI and PBI/CNT films [35].

Methanol permeabilities through the membranes were measured for 1 M methanol at 60 °C. A side-by-side diffusion cell consisting of two-compartment glass reservoirs (source and receiving reservoirs) was used to test the permeability. The source reservoir was filled with an aqueous methanol solution and the receiving reservoir was filled with DI water. These two reservoirs were separated by the membrane under test. The methanol concentration transported through the membranes was determined by sampling a small amount of the solution from the receiving compartment at time intervals for concentration measurement using a density/specific gravity meter (model DA-130N, Kyoto Electronics Manufacturing Co. Ltd., Kyoto, Japan). The methanol permeability was calculated as the slope of the concentration increase with elapsed time multiplied by the source reservoir volume and film thickness, followed by division of the effective diffusion membrane area and initial methanol concentration in the source reservoir [30,36].

2.5. Water and methanol uptakes and water diffusivity

The water uptake in the membrane was determined by measuring the difference between the dry weight (W_o, g) and total weight (W_t, g) after immersion in 60 °C DI water. The solvent uptake (M) was calculated from the following equation [37,38]:

$$M = \frac{W_t - W_o}{W_o} \tag{1}$$

In the following equation, M_t and M_∞ denote the water uptake at time t and after the sorption reached a steady state (which represents equilibrium uptake). The methanol equilibrium uptake in the film was also measured using a similar procedure to that for water uptake, except that pure methanol was used as the solvent.

The water diffusion coefficient was calculated using the initial slope method on the sorption data during the transient regime [39]. The methanol uptakes at various elapsed times prior to reaching sorption equilibrium were recorded. The diffusion coefficient was fitted for a relative uptake data set as a function of time [40,41]:

$$\left(\frac{M_t}{M_\infty}\right)^2 = \frac{16Dt}{\pi\delta^2} \tag{2}$$

where M_t and M_∞ are the solvent uptake (in g g^{-1}) at time t and at equilibrium, respectively, D is the diffusion coefficient and δ is the membrane thickness.

2.6. Alkali doping and electrolyte conductivity

To prepare the hydroxide-conducting electrolytes for fuel cells the PBI and PBI–CNT composite membranes were immersed in a 6 M KOH solution for 6 days. The KOH uptakes in the membranes were calculated using Eq. (1). The thickness increase upon alkali doping was determined as the thickness difference prior to and after doping divided by the dry film thickness. The alkali-doped electrolyte was sandwiched between two stainless steel electrodes with a working area of 1.33 cm^2 in a T-shaped glass holder [11]. The glass holder was placed in a chamber with constant temperature and humidity (60 °C, relative humidity of 99%). The two ends of the electrodes protruding from the glass holder were connected to the working and assistant electrodes of a potentiostat (Autolab PGSTAT-30, Eco Chemie B.V., Utrecht, Netherlands). The alternating current (AC) impedance measurements were obtained with a scan range of 100 kHz–100 Hz and an excitation signal of 10 mV. The impedance data were represented in a Nyquist plot. The electrolyte bulk resistance (R_E) was calculated from the intercept on the real axis of the Nyquist plot [11]. The conductivity (σ) was calculated according to the following equation:

$$\sigma = \frac{L}{R_E A} \tag{3}$$

where L is the electrolyte thickness (cm), and A is the working area (1.33 cm^2) of the stainless steel electrode.

2.7. Cell performance measurement

2.7.1. Gas diffusion electrodes prepared in-house

The catalyst (Pt/C or Pt–Ru/C) was mixed with 5 wt% Nafion ionomer solution (Du Pont, Wilmington, DE, USA), DI water, and isopropanol under ultrasonication for at least 15 min to obtain well-dispersed catalyst slurry. Appropriate amounts of anode or cathode slurry were sprayed onto a 5-cm^2 gas diffusion layer (GDL) (W0S1002, 0.36-mm carbon cloth, without a micro-porous layer, from CeTech Co., Ltd., Taichung, Taiwan) using a spray gun (model GP-2, Fuso Seiki Co., Ltd., Tokyo, Japan). During the catalyst deposition, the nitrogen pressure into the spray gun was set at 13.8 kPa (2 psi) to prevent the ink from penetrating through the GDL. In order to form a uniform layer, catalyst was sprayed from side to side in a steady motion to ensure that the same amount of catalyst was deposited on the entire 5 cm^2 area of the GDL. After each spraying round, the wet catalyst was blow dried with a low flow rate of unheated air for 30–60 s and the resulting GDE thickness was approximately 0.46 mm. When the spraying was completed, the catalyzed GDL was placed in an oven at 60 °C for 3 h. The catalyst loads were 5.0 mg cm^{-2} on both anode and cathode electrodes.

2.7.2. Fuel cell performance measurement

The alkali-doped electrolyte was sandwiched between the anode and cathode GDEs to fabricate the membrane electrode assembly (MEA) with the GDEs' catalyst layers facing the electrolyte membrane. The GDEs were Pt–Ru/C for the anode and Pt/C for the cathode. The GDEs from E-tek and those prepared in-house were tested. The active area of the MEA was 5 cm^2.

To assemble the ADMFC, two Teflon gaskets with a hollow area of 2.3 cm × 2.3 cm were used to surround the MEA. Two flow plates (thickness of 2 mm) made of high-density graphite with carved serpentine flow channels (1 mm wide and 1 mm deep) were in contact with the gaskets. Gold-plated copper end plates (thickness of 10 mm) were fixed next to the flow plates and served as current collectors. The single cell assembly was finally bolted and screwed using a torque wrench with a force of 35 Torr. The experimental set-up was illustrated in our previous work [30,42]. The fuel (1 M methanol/6 M KOH or 2 M methanol/6 M KOH) was maintained at 60 or 90 °C in a thermostatic chamber and recirculated through the anode compartment at a flow rate of 5 mL min^{-1}. The cathode feed, oxygen gas, was humidified by passing through a bubbler with a flow rate of 100 cm^3 min^{-1}. The ADMFC electrochemical measurements were recorded using a constant current density mode with an electrical load (PLZ164WA electrochemical system, Kikusui Electronics Corporation, Tokyo, Japan). The DMAFC cell voltage (V) was obtained by varying the current at 5-mA intervals and equilibrated for 7 s between the intervals during the polarization curve measurement. The power density (P) was calculated as the product of the cell voltage and the current density (I). The power density was plotted as a function of the current density (P–I curve) to determine the peak power density (P_{max}) under the tested condition.

3. Results and discussion

3.1. Physico-chemical characteristics of PBI/CNT composites

The prepared PBI film exhibited a smooth top surface and dense structure (Fig. 1(a) and (b)) with a film thickness of 50 μm. The PBI-functionalized MWCNT had a coarse surface (Fig. 1(c)) as the polymer was grafted onto the MWCNT outer layer. The graft yield was approximately 25% by weight. As the functionalized MWCNT was incorporated into the PBI matrix, the resulting film showed some roughness due to the presence of the CNT (Fig. 1(d)).

The FTIR spectra of the PBI and PBI/CNT are illustrated in Fig. 2. The PBI sample exhibited significant peaks at wavenumbers of 1293, 1540, and 1640 cm^{-1} (caused by the imidazole ring and C–N stretching). The broad peaks at 3150 and 3410 cm^{-1} were related to the N–H bonds. As more CNT was added in the PBI, a lower signal was released from the sample. Moreover, all samples demonstrated a strong XRD peak at 2θ of 26° (Fig. 3), implying that these membranes exhibited crystalline regions [43].

The thermal stability of PBI composites containing 0–1% CNT loaded membranes was studied with thermal gravimetric analyses. The results are shown in Fig. 4. The pure PBI displayed a high thermal stability. The decomposition temperature of PBI and the PBI composites containing 0.05–1% (PBI–0.05CNT, PBI–0.1CNT, PBI–0.15CNT, and PBI–1CNT) were 645, 672, 693, 703, and 707 °C,

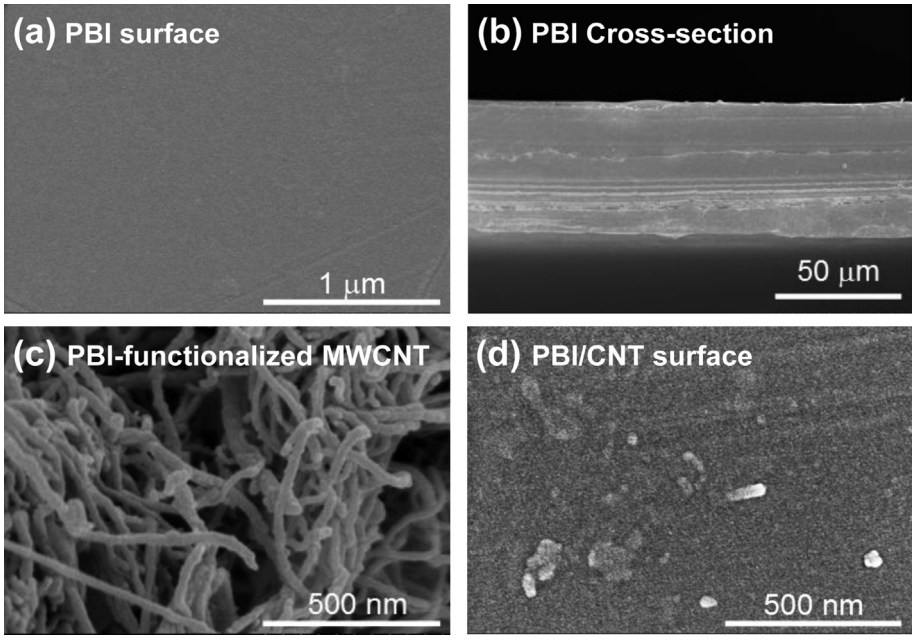

Fig. 1. Scanning electron micrographs of (a) top surface of PBI, (b) PBI cross-section, (c) PBI-functionalized MWCNT, and (d) top surface of PBI/CNT composite film.

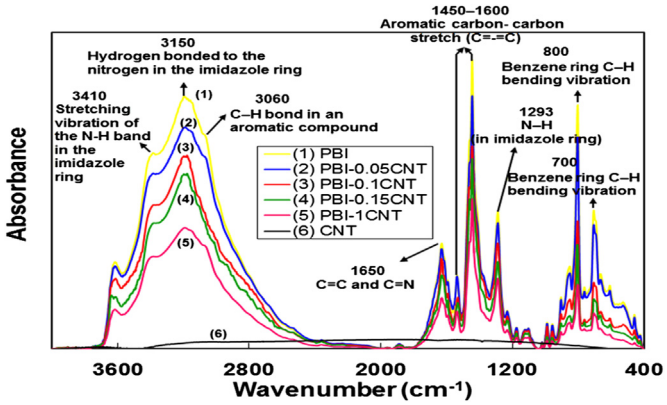

Fig. 2. FTIR spectra of PBI, CNT, and PBI/CNT composites containing various CNT loadings (0.05–1%).

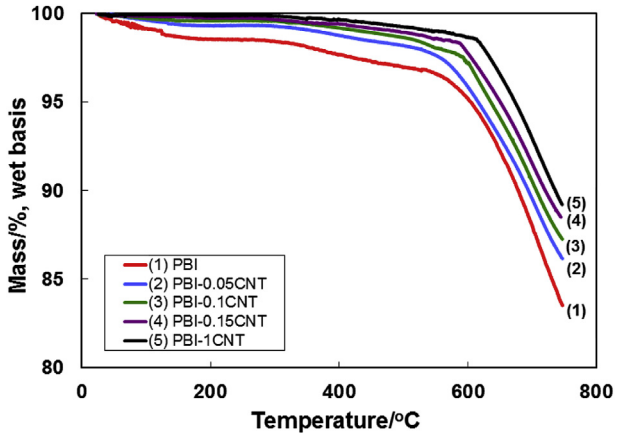

Fig. 4. Thermal gravimetric analyses on PBI composites containing 0–1% CNT loading.

respectively (Table 1). Addition of 0.05–1% CNT into the PBI matrix significantly increased the decomposition temperatures of the nanocomposites by 27–62 °C. The results all indicate that the thermal stability of PBI membranes could be increased by increasing the CNT content.

The pure PBI film had an average tensile stress of 62.7 MPa (Table 1). The tensile stress of the PBI/CNT nanocomposites varied from 41 to 96.6 MPa. The Young's modulus ranged from 13.8 to 30.8 MPa for all PBI and PBI/CNT samples. It appeared that the PBI/CNT composites had sufficient strength for the fuel cell application.

3.2. Hydrophilicity and transport properties in PBI/CNT

The contact angle of the PBI/CNT composites slightly increased from $64.33 \pm 1.41°$ to $69.09 \pm 1.25°$, which might have been due to a rougher surface on the CNT-containing films (Fig. 1(d)) or a more hydrophobic top surface upon CNT addition [44,45]. Fig. 5 shows the water uptake for the PBI/CNT membranes containing 0–1% CNT. The equilibrium water uptake of PBI/CNT membranes increased with CNT loading in the PBI composition. In the pristine PBI film, approximately 17.5 g of water was sorbed into 100 g of dry PBI membrane, equivalent to 2.9 water molecules per repeating PBI molecular. In a comparison with the water uptakes in other PBI studies, our data are consistent with literature values of 15–19 g per 100 g [16,31,46,47]. In the PBI composite containing 1% CNT, the water uptake increased to 21.5 g per 100 g dry film, which is 23% higher than the water uptake in the pure PBI membrane, and was equivalent to 3.6 water molecules per repeating PBI molecular unit. The CNTs in the polymeric matrix may have disrupted the polymer crystal alignment and increased the amorphous region [42].

The water sorption history was used to calculate the water diffusion coefficient (Eq. (2)) and the results are summarized in Table 1. The water diffusion coefficients in PBI, PBI–0.05CNT, PBI–0.1CNT, PBI–0.15CNT, and PBI–1CNT were 1.084×10^{-13}, 1.189×10^{-13}, 1.204×10^{-13}, 1.311×10^{-13}, and 1.201×10^{-13} $m^2\ s^{-1}$, respectively. This water diffusion coefficient in the PBI was in agreement with the value (0.95×10^{-13} $m^2\ s^{-1}$) reported by Shi et al. [48]. The diffusion coefficient values increased slightly with the CNT content. The increased water diffusivity in the PBI/CNT composites may result from a less crystallized polymer region, as indicated in the higher fractional free volume in the CNT-containing samples (Table 1). This increased polymer free volume was beneficial for water retention and hydroxide ion diffusion [28,29]. Meanwhile, the micro-channel provided by the functionalized CNT also facilitated water transport along the CNT surface [7,28,29].

The methanol permeability of PBI and PBI/CNT membranes were measured with a 1 M methanol solution at 60 °C. The permeated methanol concentration through the membrane as a function of time is illustrated in Fig. 6, and the permeability results are listed in Table 1. The methanol permeability decreased monotonically from 2.59×10^{-10} to 1.85×10^{-10} $m^2\ s^{-1}$, with CNT loading increasing from 0 to 1%. Similar decreases in methanol permeability were reported for PVA/fume silica, PVA/CNT, and PVA–FeCNT nanocomposites [7,28,49]. The methanol permeability in PBI is similar to that of Nafion (2.3×10^{-10} $m^2\ s^{-1}$ [50]) and sulfonated polystyrene-block-poly(ethylene-ran-butylene)-block-polystyrene copolymer of 47% degree of sulfonation (2.6×10^{-10} $m^2\ s^{-1}$ [51]). Although the polymeric fractional free volume was higher in the PBI/CNT composite than that for the PBI, the enlarged free volume radius (2.62 Å) was sufficient for both hydroxide (radius of 1.1 Å [52]) and water (kinetic diameter of 2.641 Å [53]) transport but methanol molecules (with kinetic diameters of 3.8–4.1 Å [54]) had limited access. Several researchers have reported suppressed methanol permeability after nano-particles or CNTs were added into polymeric films [7,27,31,55,56]. The competition in the transfer path favored the diffusion of the smaller permeants.

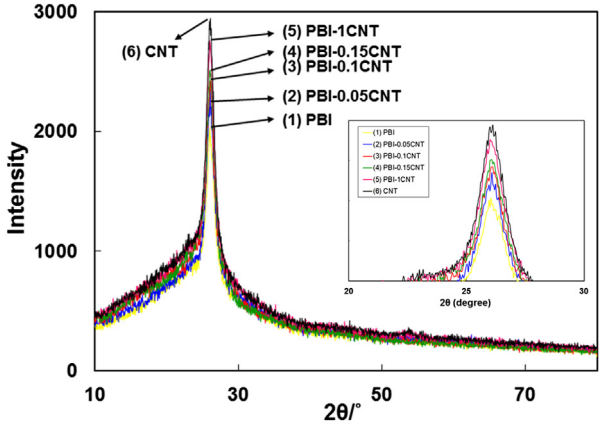

Fig. 3. X-ray diffraction patterns of PBI and PBI/CNT composites (0–1% CNT loadings).

3.3. KOH-doped PBI/CNT characteristics

The total alkaline uptakes of the membranes in 6 M KOH were measured at 60 °C and the data are shown in Table 1. The PBI-based

Table 1
Characteristics of PBI and PBI/CNT composites.

Composite films	PBI	PBI–0.05CNT	PBI–0.1CNT	PBI–0.15CNT	PBI–1CNT
Decomposition temperature (°C)[a]	645	672	693	703	707
Tensile stress (MPa)	62.7 ± 17.4	56.4 ± 24.5	53.5	41.0	96.6 ± 32.8
Contact angle (degree)[b]	64.33 ± 1.41	66.31 ± 0.33	66.71 ± 0.34	66.96 ± 0.70	69.09 ± 1.25
Water uptake (%)[c]	17.48	20.77	20.82	20.90	21.48
Water diffusion coefficient (10^{-13} m^2 s^{-1})[c]	1.08 ± 0.24	1.19 ± 0.36	1.20 ± 0.44	1.31 ± 0.42	1.20 ± 0.46
Relative fractional free volume (%)	2.21 ± 0.06	2.47 ± 0.05	–[d]	–	2.44 ± 0.05
Methanol uptake (%)[c]	12.47	14.69	16.06	17.59	21.08
Methanol permeability (10^{-10} m^2 s^{-1})[e]	2.59	2.58	2.35	2.11	1.85
Alkali uptake (g g^{-1})[f]	1.10	1.01	–	–	1.07
Thickness increased (%)[f]	104	77	–	–	72
Conductivity (S cm^{-1})[f]	0.023	0.026	0.026	0.027	0.035

[a] Temperature at 5% weight loss.
[b] Mean ± standard deviation ($n = 5$).
[c] Dry mass basis at 60 °C.
[d] Not determined.
[e] At 1 M methanol at 60 °C.
[f] Doped with 6 M KOH at 60 °C; thickness increase is calculated as (wet film thickness − dry film thickness)/dry film thickness × 100%.

films absorbed a substantial amount of KOH solution, as the dry film mass took up at least its own weight in KOH and water constituents. Compared with DI water uptakes of 17.5–27.5% (dry basis) in the membranes, the surprisingly high alkaline uptake could be due to the strong interaction (hydrogen bonding and/or neutralization [25,27]) between KOH and the PBI molecules, in addition to the simple physical partition effect of KOH into the water-swollen membranes. The relative thickness changes in the KOH-doped films are also shown in Table 1. The thickness increase in the PBI, PBI/0.05CNT, and PBI/1CNT membranes were approximately 104, 77, and 72% increases in the membrane thickness compared with the dry films, respectively. The thickness increase demonstrates a slightly declining trend with respect to the CNT loading. The small dimensional change may be associated with the restricted chain flexibility caused by CNT addition.

The alkali-doped electrolyte conductivities were measured at 60 °C and the results are summarized in Table 1, along with the sorption and diffusion characteristics of the PBI and PBI/CNT membranes. The CNT-containing electrolyte exhibited a higher ionic conductivity (0.026–0.035 S cm^{-1}) than the pristine PBI (0.023 S cm^{-1}, which was identical to the value reported by Hou et al. [27] and Huang et al. [57]). These data are in the same order of magnitude as the KOH-doped PVA electrolytes [28,49] and comparable to Nafion conductivity [58,59]. Xing and Savadogo reported that the KOH-doped PBI reached a maximum conductivity of 0.04 S cm^{-1} at 25 °C when PBI of 40 μm in thickness had been doped in 6 M KOH for 10 days [60]. Our data were in close to their value although a shorter doping time (6 days) was applied.

Ionic conductance is carried out via many mechanisms: Grotthus (hopping), vehicular (bulk) diffusion, and surface diffusion [61]. In addition to having higher pure water uptakes and higher water diffusivity coefficients (Table 1) than the PBI film, PBI/CNT films might be beneficial for ionic transport via the hopping mechanism. The PBI/CNT film also exhibited a higher free volume level than the PBI sample (Table 1), which might have induced increased ionic diffusion within the electrolytes (via vehicular diffusion) and enhanced conductivity. In addition, the PBI-functionalized CNT also provided fast micro-channels for hydroxide and water transports (via surface diffusion) and raised ionic conductance. All these factors contributed to the higher conductivities in the PBI/CNT films compared to the PBI films.

3.4. Effect of CNT addition on fuel cell performance

Fig. 7 shows the polarization curves for the ADMFCs using the PBI and PBI/CNT electrolytes with 1 M methanol in 6 M KOH at 90 °C. The PBI containing 0.05% CNTs (PBI/0.05CNT) had a higher open-circuit voltage (V_{oc}) (0.75 vs. 0.6 V) and peak power density (50.9 vs. 24.5 mW cm^{-2}) than the PBI electrolytes. As the current

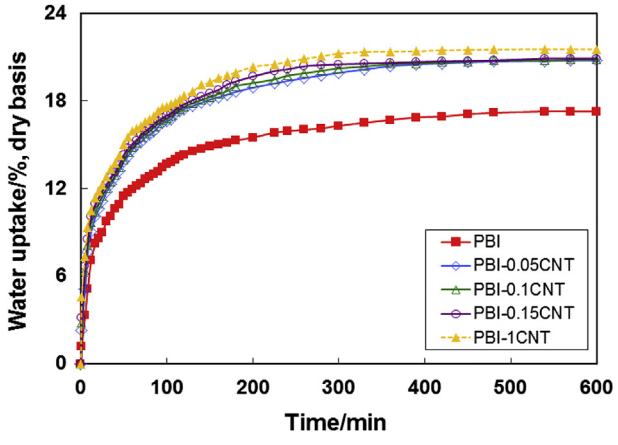

Fig. 5. Water sorption (grams per 100 g dry film) history into PBI and PBI/CNT composites at 60 °C.

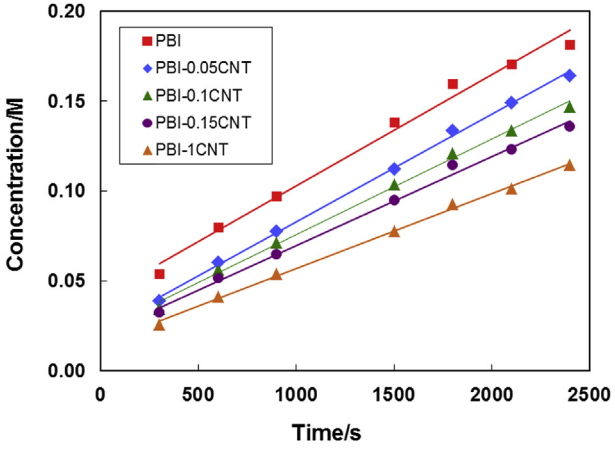

Fig. 6. Methanol concentration in receiving reservoir through PBI and PBI/CNT composites at various elapsed times (volume of donor and receiving reservoirs: 30 mL, membrane area: 1 cm^2, temperature: 60 °C).

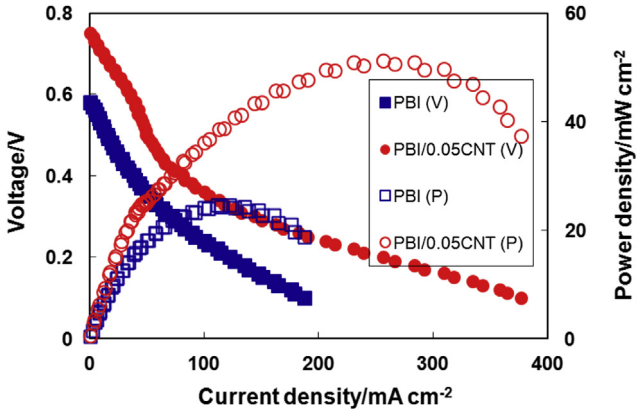

Fig. 7. Cell voltage (left axis) and power density (right axis) of ADMFCs with KOH-doped PBI and PBI/CNT electrolytes. The cells were fed with 1 M methanol in 6 M KOH at a flow rate of 5 mL min^{-1}, humidified oxygen gas at a flow rate of 100 mL min^{-1}, operated at 90 °C. The catalysts were Pt–Ru (5 mg cm^{-2}, from E-tek) and Pt (5 mg cm^{-2}, from E-tek) for anode and cathode, respectively. Both E-tek GDEs were treated with a PTFE hydrophobic layer.

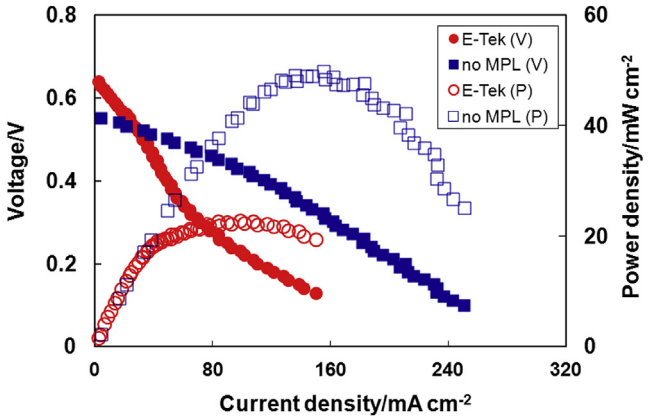

Fig. 8. Cell performance comparison between E-tek GDEs and prepared in-house GDEs. The cell voltage is on the left axis and the power density on the right axis. The ADMFCs were equipped with KOH-doped PBI/0.05CNT electrolyte, fed with 1 M methanol in 6 M KOH at a flow rate of 5 mL min^{-1}, humidified oxygen gas at a flow rate of 100 mL min^{-1}, and operated at 60 °C. The catalyst loadings were 5 mg cm^{-2} for Pt–Ru (1:1, anode) and Pt (cathode).

density increased, differentiation within the fuel cell potential became significant. The CNT surface was functionalized with the PBI chains to increase its chemical compatibility with the polymer matrix for the film formation process, and the functionalized PBI layer may have enhanced the intrinsic ionic conduction after alkali doping. Moreover, the polybenzimidazole containing 0.05% CNTs demonstrated a higher relative fractional free volume compared to the pristine PBI, as shown in Table 1. The higher free volume significantly facilitates the transfer of hydroxide ions in the PBI/0.05CNT electrolyte membrane with respect to that in the PBI film [33,49]. These results demonstrate that the functionalized CNTs can achieve good compatibility with the PBI matrix and increase the polymer free volume. These effects are beneficial for improving the full cell performance using the PBI/0.05CNT composite rather than the PBI film. The addition of a very small amount of the functionalized CNT can significantly improve the ionic conductivity and the fuel cell performance.

3.5. Performance comparison on different GDEs

The ADMFC performances using the PBI/0.05CNT electrolyte with E-tek GDEs and home-made GDEs were compared while using 1 M methanol in 6 M KOH fuel and operating at 60 °C. The E-tek GDEs were treated with a PTFE hydrophobic layer while the home-made GDEs were used without PTFE treatment. These GDEs all had catalyst loadings of 5 mg cm^{-2} for both the anode (Pt–Ru/C) and cathode (Pt/C). The polarization curves in Fig. 8 demonstrate that the E-tek GDEs produced a higher V_{oc} than the home-made ones, most likely due to the resistance to methanol transfer offered by the barrier of the hydrophobic layer. This effect was especially pronounced in the low current density region: the fuel utilization efficiency was low (less than 1%, which was calculated as 30 mA cm^{-2} × 5 cm^2/(96,485 C mol^{-1})/6/(5 mL × 1 mol L^{-1}/60 s)), and a significant amount of un-reacted methanol could cross-over to the cathode if the GDEs were not treated with PTFE [29]. In the higher current density region, however, the fuel was better utilized and the methanol cross-over issue was not that severe even without PTFE treatment. Moreover, the carbon paper (gas diffusion layer) in the home-made GDEs allowed smooth transport of reactants, including methanol, hydroxide ions, moisture, and oxygen. The carbon dioxide gas produced on the anode was easily dissolved in the alkaline solution and was readily removed via the gas diffusion layer [62]. The lack of a PTFE layer also reduced the electrical resistance in the home-made GDEs. Therefore, higher cell voltage values were observed for the home-made GDEs at current densities over 30 mA cm^{-2}. The peak power density for the home-made GDEs doubled those with the E-tek (49.9 vs. 22.7 mW cm^{-2} at 60 °C, Fig. 8).

3.6. Effects of cell temperature and methanol concentration

Fig. 9(a) shows the fuel cell performance at different temperatures using home-made GDE, where the anode was fed with 1 M methanol in 6 M KOH. This cell achieved a maximum power density of 49.9 and 81.3 mW cm^{-2} at 60 °C and 90 °C, respectively. The cell potential and the power density increased with increasing operating temperature because of the favored catalytic kinetics [63,64] and the higher electrolyte conductivity at higher temperatures. Higher temperatures accelerated the methanol oxidation reactions at the electrodes and resulted in a higher V_{oc} (Fig. 9(a) and (b)). Less ohmic loss was reported at the electrolyte membrane and at the interfaces at higher temperatures [33] as we found out that PBI films containing 0–1% CNT exhibited ionic conductivities of 0.21–0.27 S cm^{-1} at 30 °C and 0.23–0.35 S cm^{-1} at 60 °C. Therefore, the single cell resistance decreased as the temperature increased. In addition, lower methanol permeability was observed at 90 °C than that at 60 °C (1.07×10^{-10} vs. 2.58×10^{-10} m^2 s^{-1} from 1 M methanol solution) probably due to film shrinkage upon heating. As a result, the fuel cell performance was improved due to faster electrochemical kinetic reaction rates, less electrical resistance, and suppressed methanol permeability in the fuel cell.

Fig. 9(b) shows the dependence of cell performance on different temperatures when feeding 2 M methanol at the anode. The peak power density was 67.1 mW cm^{-2} at 60 °C and 104.7 mW cm^{-2} at 90 °C. The higher operating temperature favored the cell performance due to the improved electrode reactions, cell conductance, and the lowered fuel cross-over as aforementioned. As the methanol concentration was increased from 1 to 2 M, the methanol permeability was decreased by 49–59% and the cell was able to operate at higher current density and the power density output was improved by 29–34% at 60–90 °C. The good methanol barrier property of the PBI-based membrane enabled a thin film (50 μm in this work) to be employed in the fuel cell, resulting in low overall cell resistance. Furthermore, the fuel cell performance was greatly

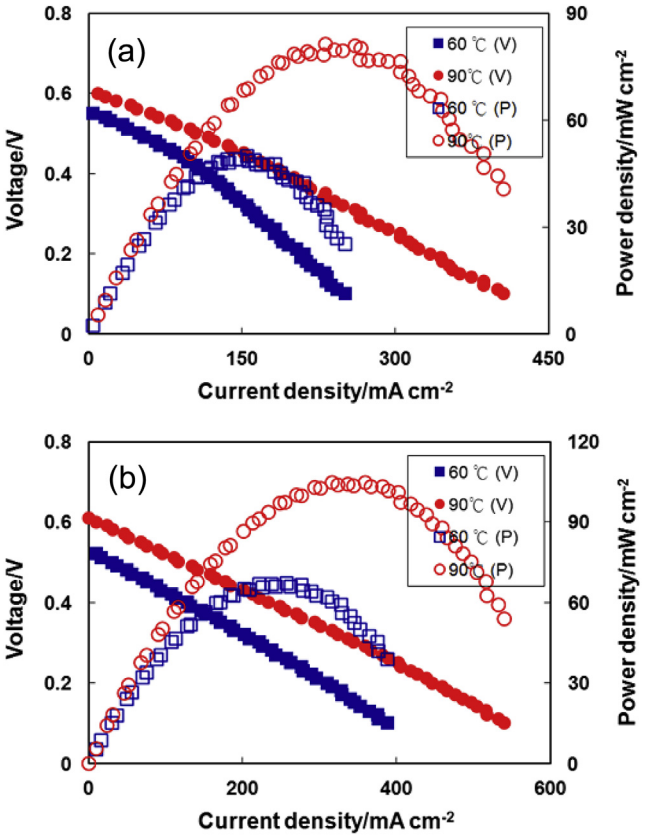

Fig. 9. Temperature effect on fuel cell voltage (filled symbols, left axis) and power density (open symbols, right axis) for ADMFCs fed with (a) 1 M and (b) 2 M methanol in 6 M KOH (anode fuel at a flow rate of 5 mL min^{-1}, humidified oxygen gas at a flow rate of 100 mL min^{-1}, with KOH-doped PBI/0.05CNT electrolytes, GDEs prepared in-house with Pt–Ru (5 mg cm^{-2}) and Pt (5 mg cm^{-2}) for the anode and cathode, respectively).

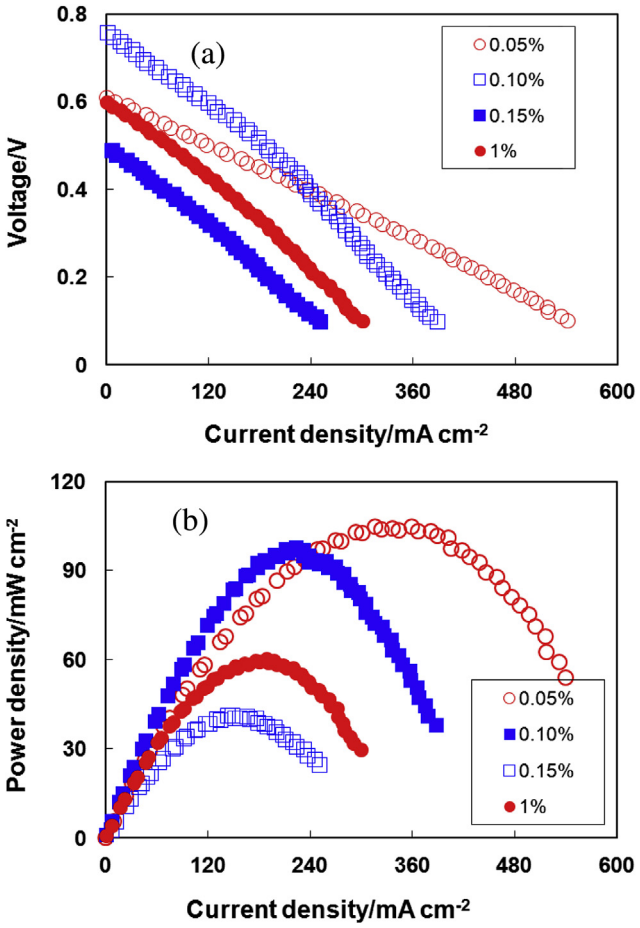

Fig. 10. Effect of CNT content in PBI on (a) cell voltage and (b) power density at 90 °C. The cell were fed with 2 M methanol in 6 M KOH at a flow rate 5 mL min^{-1}, humidified oxygen at a flow rate of 100 mL min^{-1}, with GDEs prepared in-house. The catalyst loadings were 5 mg cm^{-2} for Pt–Ru (1:1, anode) and Pt (cathode).

enhanced at an elevated temperature (90 °C) using this thermally stable PBI composite.

3.7. CNT loading effect

Several CNT loadings in PBI were prepared to evaluate their effect on the ADMFC cell performance. Fig. 10 shows the cell performance where the fuel cells were fed with 2 M methanol in 6 M KOH at 90 °C. With the electrolyte containing 0.05% CNT, the V_{oc} was 0.6 V and the ohmic resistance was 4.5×10^{-3} Ω cm^2 (which was calculated from the slope of the ohmic region in the polarization curve) for a single fuel cell. As the CNT loading doubled to 0.1%, the V_{oc} increased to 0.8 V and the ohmic resistance was 8.5×10^{-3} Ω cm^2. The cell voltage using the 0.1% CNT was higher than that with 0.05% CNT at a current density below 240 mA cm^{-2} but was lower at higher current densities (Fig. 10(a)). With the CNT content increasing to 0.15–1%, the V_{oc} decreased to 0.5–0.6 V and the ohmic resistance was 8×10^{-3}–8.5×10^{-3} Ω cm^2. Both the fuel cell voltage and the power density dropped significantly from those with 0.05% or 0.1% CNT loading (Fig. 10). Overall the 0.05% CNT-containing electrolyte exhibited the highest peak power density among the tested samples (Fig. 10(b)).

This optimal CNT loading of 0.05% was consistent with previous research [27,33], except that in a polyvinyl alcohol/Fe_3O_4–CNT composite, in which 0.15% CNT loading was found to be optimal [49]. The effect of the CNT content on the fuel cell performance can be explained in terms of many electrolyte characteristics. First of all, the incorporation of CNTs resulted in a higher free volume compared to the pure PBI film (Table 1), and the fractional free volume was positively related to water diffusivity and the hydroxide ion transfer through the PBI matrix. However, the free volume might be reduced beyond a certain level of CNT content because the CNTs tend to form aggregates and constrain molecular motion [65]. When more CNTs were added to the polymer, the enhanced hydroxide ion transport in the CNT channel and the PBI matrix was offset by the more tortuous path in the CNT channel and the decreased free volume in the polymer matrix. Although the film conductivity increased with CNT content (Table 1), the fuel cell voltage and power density dropped significantly (Fig. 10).

The interfacial contact between the electrolyte and the GDEs may also play a role in the single cell performance. The pristine PBI film exhibited smooth top surface and dense structure (Fig. 1(a) and (b)) with a film thickness of 50 μm. The PBI-functionalized CNT demonstrated a rough surface (Fig. 1(c)) as the polymer was grafted onto the CNT outer layer. As the functionalized CNT was incorporated in the PBI matrix, the resulting film showed some roughness due to the presence of the CNT (Fig. 1(d)). This surface might have caused incomplete contact with the GDEs and created increased interfacial electrical resistance. The ohmic over-potentials (as shown in the slopes of the polarization curves in Fig. 10(a)) increased as the CNT content exceeded 0.05%. Therefore, in addition

to the physical and electrical properties of the electrolyte as aforementioned, an optimal CNT loading is closely related to the elasticity (flexibility) of the solid electrolyte and the interfacial contact with other adjacent components. More investigation on the effects of nano-fillers on polymeric composite properties and their impacts on fuel cell performance is highly advocated.

3.8. Cell performance comparison with literature data

The literature data on the peak power densities for ADMFCs at comparable operating conditions are summarized in Table 2. Using the PVA-based electrolytes, the peak power densities for 30 °C were in the range of 15–36 mW cm^{-2} [11,29,49]. As the temperature was raised to 60 °C, the peak power densities increased to 40–88 mW cm^{-2} [11,29,49]. The PVA composites (with decomposition temperatures of 241–250 °C [49]) were not as thermally stable as the PBI-based materials (with decomposition temperatures of 645 °C and above, Table 1). When the ADMFC was fed with 2 M methanol in 6 M KOH (as the anode fuel) and humidified oxygen (as the cathode feed), the KOH-doped PBI/0.05CNT could achieve a maximum power density of 104.7 mW cm^{-2} at 90 °C. To the best of our knowledge the obtained P_{max} at 90 °C is the highest value reported in the DMAFC literature (Table 2).

Table 2
Comparison of the peak power densities of ADMFCs reported in the literature.[a]

Electrolyte	Cell temperature (°C)	Peak power density (mW cm^{-2})	Source
KOH-doped PVA[b]	30	24.7	Lue et al. [49]
KOH-doped PVA/FS[c]	30	15.0	Lue et al. [11]
KOH-doped PVA/CNT[d]	30	25.8	Lue et al. [27]
KOH-doped PVA/FeCNT[e]	30	35.7	Lue et al. [49]
KOH-doped ETFE[f]	60	4.2[g]	Varcoe and Slade [15]
KOH-doped PVA	60	6.0[h]	Fu et al. [13]
KOH-doped PVA	60	36.5	Lue et al. [49]
KOH-doped PVA/FS	60	39.0	Lue et al. [11]
KOH-doped PVA/CNT	60	68.1	Lue et al. [27]
KOH-doped PVA/FeCNT	60	87.8	Lue et al. [49]
KOH-doped PBI/CNT	60	67.1	This work
KOH-doped PVA/PAADDA/PEG[j]	70	15.4[i]	Zhou et al. [14]
KOH-doped ETFE[f]	80	8.5[g]	Varcoe and Slade [15]
KOH-doped PVA	90	10.2[h]	Fu et al. [13]
KOH-doped PBI[k]	90	31.0[l]	Hou et al. [24]
KOH-doped PBI/CNT	90	104.7	This work

[a] Anode: Pt–Ru (5 mg cm^{-2}) fed with 2 M methanol in 6 M KOH; cathode: Pt (5 mg cm^{-2}) fed with humidified oxygen (at 1 bar). Operating conditions other than this are shown in the following table footnotes.
[b] PVA: polyvinyl alcohol.
[c] FS: fumed silica (SiO_2).
[d] CNT: carbon nano-tubes (pre-functionalized with the polymer as the main composition to which the CNT is incorporated).
[e] FeCNT: carbon nano-tubes (pre-functionalized with polymer) containing Fe_3O_4 pedant nano-particles.
[f] ETFE: quaternary-ammonium-functionalized poly(ethylene-co-tetrafluoroethylene).
[g] Anode: Pt–Ru (4 mg cm^{-2}) fed with 2 M methanol; cathode: Pt/C (4 mg cm^{-2}) fed with oxygen at a back-pressure of 2.5 bar.
[h] Anode: Pt/C (1 mg cm^{-2}) fed with 2 M methanol in 2 M KOH; cathode: Pt/C (1 mg cm^{-2}) fed with oxygen at a flow rate of 20 mL min^{-1}.
[i] Anode: Pt/C (0.8 mg cm^{-2}) fed with 2 M methanol in 2 M KOH; cathode: Pt/C (2.5 mg cm^{-2}) fed with oxygen at a flow rate of 30 mL min^{-1}.
[j] PAADDA: poly(acrylamideco-diallyldimethylammonium chloride); PEG: poly(-ethylene glycol).
[k] PBI: polybenzimidazole.
[l] Anode: Pt–Ru (2 mg cm^{-2}) fed with 2 M methanol in 2 M KOH; cathode: Pt (1 mg cm^{-2}) fed with pressurized oxygen (0.2 bar).

4. Conclusion

In this research, KOH-doped PBI/CNT nanocomposites were prepared for alkaline direct methanol fuel cell application. The thermal stability was enhanced after incorporating 0.05–1% PBI-functionalized CNT into the PBI matrix. The methanol permeability was reduced with CNT loading. The ionic conductivity of the KOH-doped PBI/CNT was higher than that of the KOH-doped PBI. The polymeric fractional free volume was slightly increased in the CNT-containing sample. The home-made GDEs were prepared on untreated carbon cloth (without hydrophobic layer) and yielded a higher peak power density than that obtained with commercial E-tek GDEs. A high power density of 104.7 mW cm^{-2} was achieved at a 0.05% CNT loading in the PBI/CNT composite for the fuel cell fed with 2 M methanol in 6 M KOH, which was equipped with the home-made GDEs and operated at a temperature of 90 °C.

Acknowledgements

We thank the National Science Council of Taiwan for financial support (NSC 100-2221-E-182-041and NSC 101-2221-E-182-064-MY2) and R&D Center for Membrane Technology of Chung Yuan University for PALS analysis. We also extend our thanks to Dr. C.M. Shih and Ms. G.Y. Lin (Chung Gung University) for their help with the manuscript preparation and proof-correcting.

References

[1] R.C.T. Slade, J.R. Varcoe, Fuel Cells 5 (2005) 187–199.
[2] S. Mollá, V. Compañ, J. Power Sources 196 (2011) 2699–2708.
[3] H.C. Cha, C.Y. Chen, J.Y. Shiu, J. Power Sources 192 (2009) 451–456.
[4] A.V. Tripković, K.D. Popović, B.N. Grgur, B. Blizanac, P.N. Ross, N.M. Marković, Electrochem. Acta 47 (2002) 3707–3714.
[5] A.V. Tripkovic, K.D. Popovic, J.D. Lovic, V.M. Jovanovic, A. Kowal, J. Electroanal. Chem. 572 (2004) 119–128.
[6] J. Prabhuram, R. Manoharan, J. Power Sources 74 (1998) 54–61.
[7] S.J. Lue, K.P.O. Mahesh, W.T. Wang, J.Y. Chen, C.C. Yang, J. Membr. Sci. 367 (2011) 256–264.
[8] J. Kim, T. Momma, T. Osaka, J. Power Sources 189 (2009) 999–1002.
[9] H. Bunazawa, Y. Yamazaki, J. Power Sources 190 (2009) 210–215.
[10] C.C. Yang, J. Membr. Sci. 288 (2007) 51–60.
[11] S.J. Lue, W.T. Wang, K.P.O. Mahesh, C.C. Yang, J. Power Sources 195 (2010) 7991–7999.
[12] C.C. Yang, S.J. Chiu, W.C. Chien, S.S. Chiu, J. Power Sources 195 (2010) 2212–2219.
[13] J. Fu, J. Qiao, X. Wang, J. Ma, T. Okada, Synth. Met. 160 (2010) 193–199.
[14] T. Zhou, J. Zhang, J. Jingfu, G. Jiang, J. Zhang, J. Qiao, Synth. Met. 160 (2010) 193–199.
[15] J.R. Varcoe, R.C.T. Slade, Electrochem. Commun. 8 (2006) 839–843.
[16] Q. Li, Solid State Ionics 168 (2004) 177–185.
[17] R. He, Q. Li, A. Bach, J. Jensen, N. Bjerrum, J. Membr. Sci. 277 (2006) 38–45.
[18] J. Lobato, P. Cañizares, M.A. Rodrigo, J.J. Linares, R. López-Vizcaíno, Energy Fuels 22 (2008) 3335–3345.
[19] R. Wycisk, J. Chisholm, J. Lee, J. Lin, P.N. Pintauro, J. Power Sources 163 (2006) 9–17.
[20] Y.L. Ma, J.S. Wainright, M.H. Litt, R.F. Savinell, J. Electrochem. Soc. 151 (2004) 8–16.
[21] Q. Li, R. He, J.O. Jensen, N.J. Bjerrum, Fuel Cells 4 (2004) 147–159.
[22] D. Aili, L.N. Cleemann, Q. Li, J.O. Jensen, E. Christensen, N.J. Bjerrum, J. Mater. Chem. 22 (2012) 5444–5453.
[23] Q. Li, J.O. Jensen, R.F. Savinell, N.J. Bjerrum, Prog. Polym. Sci. 34 (2009) 449–477.
[24] H. Hou, G. Sun, R. He, B. Sun, W. Jin, H. Liu, Q. Xin, Int. J. Hydrogen Energy 33 (2008) 7172–7176.
[25] H. Hou, G. Sun, R. He, Z. Wu, B. Sun, J. Power Sources 182 (2008) 95–99.
[26] A.D. Modestov, M.R. Tarasevich, A.Yu. Leykin, V.Ya. Filimonov, J. Power Sources 188 (2009) 502–506.
[27] H. Hou, S. Wang, Q. Jiang, W. Jin, L. Jiang, G. Sun, J. Power Sources 196 (2011) 3244–3248.
[28] W.H. Pan, S.J. Lue, Y.L. Liu, C.M. Chang, J. Membr. Sci. 376 (2011) 225–232.
[29] S.J. Lue, W.H. Pan, C.M. Chang, Y.L. Liu, J. Power Sources 202 (2012) 1–10.
[30] C.C. Huang, Y.L. Liu, W.H. Pan, C.M. Chang, C.M. Shih, H.Y. Chu, C.H. Chien, C.H. Juan, S.J. Lue, J. Polym. Sci. Polym. Phys. http://dx.doi.org/10.1002/polb.23250.
[31] Suryani, Y.L. Liu, J. Membr. Sci. 332 (2009) 121–128.

[32] R. Kannan, P.P. Aher, T. Palaniselvam, S. Kurungot, U.K. Kharul, V.K. Pillai, J. Phys. Chem. Lett. 1 (2010) 2109–2113.
[33] Suryani, C.M. Chang, Y.L. Liu, Y.M. Lee, J. Mater. Chem. 21 (2011) 7480–7486.
[34] S.J. Lue, J.S. Ou, C.H. Kuo, H.Y. Chen, T.H. Yang, J. Membr. Sci. 347 (2010) 108–115.
[35] S.J. Lue, C.L. Tsai, D.T. Lee, K.P.O. Mahesh, M.Y. Hua, C.C. Hu, Y.C. Jean, K.R. Lee, J.Y. Lai, J. Membr. Sci. 349 (2010) 321–332.
[36] S.J. Lue, H. Juang, S. Hou, Sep. Sci. Technol. 37 (2002) 463–480.
[37] S.J. Lue, S.J. Shieh, Polymer 50 (2009) 654–661.
[38] S.J. Lue, S.W. Yang, J. Macromol. Sci. Phys. 44 (2005) 711–725.
[39] S.J. Lue, S.F. Wang, L.D. Wang, W.W. Chen, K.M. Du, S.Y. Wu, Desalination 233 (2008) 277–285.
[40] S.J. Lue, J.S. Ou, S.L. Chen, W.S. Hung, C.C. Hu, Y.C. Jean, J.Y. Lai, J. Membr. Sci. 356 (2010) 78–87.
[41] S.J. Lue, T.H. Yang, K.-S. Chang, K.L. Tung, J. Membr. Sci. 415–416 (2012) 635–643.
[42] S.J. Lue, J.Y. Chen, J.M. Yang, J. Macromol. Sci. Phys. 47 (2008) 39–51.
[43] C. Xu, Y. Cao, R. Kumar, X. Wu, X. Wang, K. Scott, J. Mater. Chem. 21 (2011) 11359–11364.
[44] E.N. Konyushenko, J. Stejskal, M. Trchová, J. Hradil, J. Kovářová, J. Prokeš, M. Cieslar, J.Y. Hwang, K.H. Chen, I. Sapurina, Polymer 47 (2006) 5715–5723.
[45] F. An, C. Lu, J. Guo, S. He, H. Lu, Y. Yang, Appl. Surf. Sci. 258 (2011) 1069–1076.
[46] T.S. Chung, J. Macromol. Sci. Part C: Polym. Rev. 37 (1997) 277–301.
[47] N.W. Brooks, R.A. Duckett, J. Rose, I.M. Ward, J. Clements, Polymer 34 (1993) 4038–4042.
[48] G.M. Shi, H. Chen, Y.C. Jean, T.S. Chung, Polymer 54 (2013) 774–783.
[49] C.F. Lo, J.F. Wu, H.Y. Li, W.S. Hung, C.M. Shih, C.C. Hu, Y.L. Liu, S.J. Lue, J. Membr. Sci. http://dx.doi.org/10.1016/j.memsci.2013.05.001.
[50] B.S. Pivovar, Y. Wang, E.L. Cussler, J. Membr. Sci. 154 (1999) 155–162.
[51] J. Kim, B. Kim, B. Jung, J. Membr. Sci. 207 (2002) 129–137.
[52] Y. Marcus, J. Chem. Phys. 137 (2012) 154501-1–154501-5.
[53] R.C. Reid, J.M. Prausnitz, B.E. Poling, The Properties of Gases and Liquids, McGraw-Hill Book Co., Singapore, 1987.
[54] J.E. ten Elshof, C.R. Abadal, J. Sekulić, S.R. Chowdhury, D.H.A. Blank, Microp. Mesop. Mat. 65 (2003) 197–208.
[55] S.W. Chuang, S.L.C. Hsu, Y.H. Liu, J. Membr. Sci. 305 (2007) 353–363.
[56] S.H. Joo, C. Pak, E.A. Kim, Y.H. Lee, H. Chang, D. Seung, Y.S. Choi, J.B. Park, T.K. Kim, J. Power Sources 180 (2008) 63–70.
[57] Q.M. Huang, Q.L. Zhang, H.L. Huang, W.S. Li, Y.J. Huang, J.L. Luo, J. Power Sources 184 (2008) 338–343.
[58] Y. Sone, P. Ekdunge, D. Simonsson, J. Electrochem. Soc. 143 (1996) 1254–1259.
[59] H.L. Lin, T.L. Yu, F.H. Han, J. Polym. Res. 13 (2006) 379–385.
[60] B. Xing, O. Savadogo, Electrochem. Commun. 2 (2000) 697–702.
[61] T.J. Peckham, S. Holdcroft, Adv. Mater. 22 (2010) 4667–4690.
[62] A. Kamitani, S. Morishita, H. Kotaki, S. Arscott, J. Power Sources 187 (2009) 148–155.
[63] E.H. Yu, K. Scott, Electrochem. Commun. 6 (2004) 361–365.
[64] B.Y. Wang, H.K. Lin, N.Y. Liu, K.P.O. Mahesh, S.J. Lue, J. Power Sources 227 (2013) 275–283.
[65] W. Zhou, J. Wang, Z. Gong, J. Gong, N. Qi, B. Wang, Appl. Phys. Lett. 94 (2009) 021904-1–021904-3.